Pure Appl. Chem., Vol. 76, No. 2, pp. 321–333, 2004.

Copper(II) proteins are amenable for NMR investigations*

Ivano Bertini‡ and Roberta Pierattelli

Department of Chemistry and Magnetic Resonance Center (CERM), University of Florence, Via Luigi Sacconi 6, 50019 Sesto Fiorentino (Florence), Italy

Abstract: The possibility of investigating copper proteins by nuclear magnetic resonance is here treated. It is shown that the solution structure and dynamic information can be obtained on Type I Cu(II) proteins, which have a relatively short electron relaxation time ($\tau_S = 10^{-10}$ s). The experimental approach, in this case, is routine, although tailored for fast-relaxing nuclei.

In the case of Type II Cu(II) proteins, when the electron relaxation times are larger ($\tau_S = 10^{-8}$–10^{-9} s) and proton linewidths are broadened beyond detectable limits, heteronuclear ^{13}C spectra with direct detection can be used and the solution structure can again be obtained.

In this review, it is shown that Cu(II) proteins are now amenable for NMR investigation, the size being the only limit as in diamagnetic proteins.

INTRODUCTION

Copper is an essential element for life, and copper proteins are quite common in Nature [1,2]. Copper in proteins may be present in two oxidation states, Cu(I) and Cu(II). As copper proteins are involved in electron-transfer processes or catalyze oxidative reactions, both oxidation states are physiologically relevant, and their NMR characterization is important to the understanding of the protein function [3,4].

Cu(I) is a d^{10} metal ion and has no unpaired electrons. Therefore, its influence is limited to directly bound ligands. In any case, the relaxation features of nearby nuclei are not affected, and standard NMR experiments can be performed on Cu(I) proteins. The presence of the metal needs to be considered only when solution structural studies are performed, and information on the location and coordination geometry of the metal ion are needed. In most cases, they are derived by available structural data from solid state or extended X-ray absorption fine structure (EXAFS) [5].

When the copper ion is in the oxidized state, its presence has dramatic effects on the NMR spectra [6]. Indeed, Cu(II) is a d^9 metal ion with one unpaired electron, and consequently is paramagnetic. The magnetic moment associated with this unpaired electron exerts a non-negligible effect on the NMR parameters of nearby nuclei through hyperfine coupling. This coupling between electron and nuclear spins affects both the chemical shifts and the relaxation rates of nearby nuclei. The extent of the latter effect determines the detectability of the NMR lines of these nuclei, since NMR signal linewidths, $\Delta\nu$, are proportional to the nuclear transverse relaxation rates R_2 [7]. As a consequence, a strong influence of the electron spin on nuclear relaxation can produce broad NMR lines. In favorable cases, metal substitution allowed the detailed characterization of the metal binding site [8], but in general copper proteins have been considered for a long time not amenable for NMR spectroscopy.

*Plenary lecture presented at the 2nd Santa María Workshop on Chemistry Devoted to Bioinorganic Chemistry, Santa María del Mar, Havana, Cuba, 7–11 July 2003. Other presentations are published in this issue, pp. 321–388.

‡Corresponding author

Mononuclear copper centers in proteins may be classified into two classes [9]. Type I copper centers, typical of blue copper proteins, are characterized by the presence of a metal ion strongly bound to two His and one Cys in a distorted trigonal geometry. In addition, often a fourth weakly bound ligand (Met-S in all cases except for stellacyanin, featuring a Gln-O bound to copper) is present [10]. For this type of copper center, the relatively small energy separation between the ground and excited states provide a relatively efficient electronic relaxation mechanism, that makes the electron relaxation relatively fast ($\tau_S \approx 10^{-10}$ s) [4,11,12].

Type II copper centers are those where the copper ion has a tetragonal geometry [13]. The lack of low-energy excited states in this case implies inefficient electronic relaxation mechanisms that cause a long correlation time for the electron-nucleus interaction (τ_S in the range 10^{-8}–10^{-9} s). The dependence of nuclear transverse and longitudinal relaxation rates at high magnetic field is such that a dramatic line broadening occurs with respect to Type I copper site. The longitudinal relaxation rate R_1 decreases, instead (Fig. 1).

Proton NMR spectra and signal assignments of several oxidized Type I blue copper proteins have been reported [14–25]. These studies gave insights to the understanding of the factors influencing the electron-transfer process and allowed the first detailed structural characterization of the copper coordination sphere in solution and, eventually, to solve the first solution structure by NMR for one such a protein [26]. Type II copper proteins, instead, were and are still considered not accessible by NMR spectroscopy. However, exploiting the features of less-sensitive nuclei such as ^{13}C and ^{15}N makes it possible to obtain the signal assignment of most of the nuclei of residues that are usually inaccessible by proton NMR spectroscopy.

In a few systems where multi-copper centers are present, mixed valence states and exchange coupled centers can be found [27]. These systems display relatively sharp NMR lines due to a decreased paramagnetism or a shorter electron relaxation time, respectively [28] and have been characterized by NMR spectroscopy [29–36]. These systems will not be treated here further.

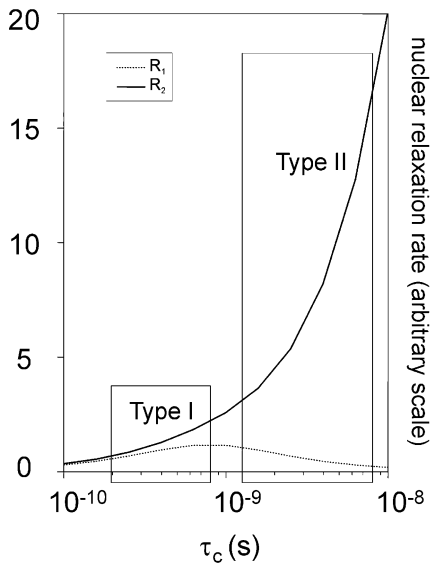

Fig. 1 Plot of the theoretical electron-nucleus dipole–dipole contribution to longitudinal (dotted line) and transverse (continuous line) relaxation rates as a function of the correlation time τ_c calculated at 16.4 T (176.1 MHz resonating frequency for carbon) by using the Solomon equation [7].

PROTON NMR SPECTROSCOPY: BLUE COPPER PROTEINS

Blue copper proteins are single domain proteins with a β-barrel fold defined by two β-sheets which can contain 6 to 13 strands following a key Greek motif (Fig. 2) [37–40]. These proteins are stable in both the reduced, Cu(I), and in the oxidized, Cu(II), forms and the metal coordination geometry is conserved in most Type I copper sites. However, different axial ligand binding motifs, which finely tune the functional properties, are found in different proteins (Fig. 3) and little structural differences do exist also within highly homologous terms of the family [10,24,41].

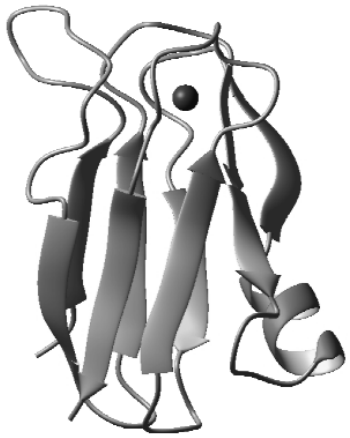

Fig. 2 Ribbon drawing of the cyanobacterium *Synechocystis sp*. PCC 6803 Cu(II) plastocyanin structure showing the secondary structure elements of the protein (PDB ID 1J5D). The metal ion is represented as a sphere of arbitrary dimension. The picture was rendered with Molmol 2.2.

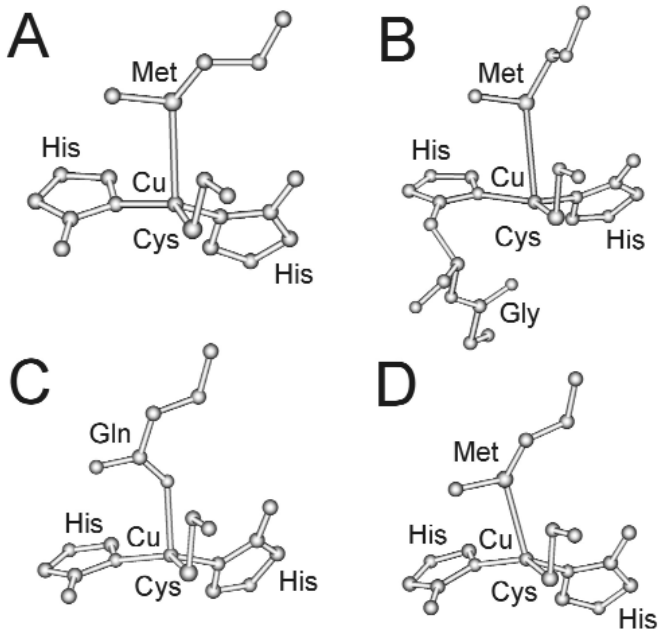

Fig. 3 Schematic drawing of the metal coordination sites in typical Type I copper proteins: (A) Plastocyanin (PDB ID 1PLC); (B) Azurin (PDB ID 4AZU); (C) Stellacyanin (PDB ID 1JER); (D) Rusticyanin (PDB ID 1RCY).

The 800 MHz ^{1}H NMR spectrum of plastocyanin, one of the best characterized blue copper proteins, is reported in Fig. 4. It shows eight downfield and two upfield hyperfine-shifted signals, which obey Curie temperature dependence (decrease in shift with temperature increasing). Only one signal (signal E) appears to be exchangeable. All hyperfine-shifted signals are characterized by very short longitudinal and transverse nuclear relaxation times.

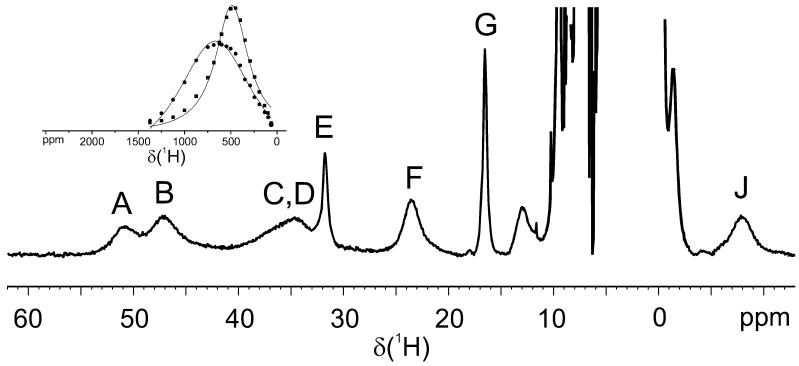

Fig. 4 800 MHz ^{1}H NMR spectra of oxidized spinach plastocyanin recorded in H_2O solution. The letters identify selected resonances whose assignment is reported in Table 1. In the insets the far-downfield regions containing signals not observable in direct detection are shown. The positions and the linewidths of these signals in the oxidized species were obtained using saturation transfer experiments over the far-downfield region by measuring the intensity of the exchange connectivity with the corresponding signal in the reduced species and performing a Lorentzian fit to the data points [19].

The general strategy for the NMR assignment of such broad resonances is based on the ability to detect NOE between nearby protons and assign them referring to a molecular model of the system investigated [42]. In some favorable cases, the assignment procedure can be simplified exploiting saturation transfer with the reduced diamagnetic species on a sample containing a 1:1 ratio of the oxidized and reduced species, as first done for amicyanin [14]. These experiments rely on the fact that the electron self-exchange rate between the two redox states in equilibrium is of the right order of magnitude to allow transfer of magnetization between a nucleus in the oxidized species and the same nucleus in the reduced species, when the former is subjected to continuous irradiation in a 1D NMR experiment. The efficiency of saturation transfer depends on the self-exchange rate between the two redox states of the protein, which, in turn, can be tuned by changing the ratio between reduced and oxidized species, temperature, pH, or ionic strength. We applied this strategy to assign all the detectable signals of plastocyanin and to locate the spectral position of NMR signals with a chemical shift of hundreds of ppm and broadened beyond detectable limits in the oxidized form, such as the signals of the Cys residue coordinated to copper [19]. For the latter, selective saturation was applied over a large spectral range (±2500 ppm) by shifting the position of the decoupler, despite the fact that no signal was observed. Indeed, if a signal broadened beyond detectable limits is present in the irradiated spectral region, saturation transfer is still operative and its effect will be maximum when the decoupler exactly matches the frequency of the broad signal. Reporting the intensity of the saturation transfer (i.e., the intensity of the signal in the diamagnetic species) vs. the chemical shift of the decoupler permits the reconstruction of the broad resonances line shape (see insets of Fig. 4). With this approach, we first assigned the complete set of hyperfine-shifted resonances in plastocyanin (Table 1) [19], followed by those of other blue copper proteins [20,22,23,26]. By comparison, the assignment of several other systems has been accomplished [24,25].

Table 1 Hyperfine shifted signals corresponding to copper ligands in Cu(II) plastocyanin [19,26], azurin [20], stellacyanin [20], pseudoazurin [23], and rusticyanin [23]. His A and His B refer to the C- and N-terminal histidine ligands, respectively. All the spectra were recorded at 800 MHz.

Signal		Spinach Plastocyanin[a]	*Synechocystis* PCC6803 Plastocyanin[b]	*Pseudomonas aeruginosa* Azurin[c]	Cucumber Stellacyanin[d]	*Achromobacter cycloclastes* Pseudoazurin[e]	*Thiobacillus ferrooxidans* Rusticyanin[f]
		δ (ppm)					
	Hβ Cys	650	610	850	450	510	240
	Hβ′ Cys	490	520	800	375	390	300
A	$H\delta_2$ His A	51.6	52.6	54.0	55.0	53.5	58.1
B	$H\delta_2$ His B	47.1	51.1	49.1	48.0	46.1	50.2
	$H\varepsilon_2$ His A	–	42.9	–	–	–	–
C	$H\varepsilon_1$ His A	35.6	38.5	46.7	41.2	32.0	36.7
D	$H\varepsilon_1$ His B	35.6	35.7	34.1	29.8	32.0	30.3
E	$H\varepsilon_2$ His B	31.4	31.1	27	26	23.0	25.3
G	Hα Asn/Ser	17.0	14.7	19.9	16.9	17.4	19.5
	ε-CH_3 Met	–	–	–	–	12.1	8.1
J	Hα Cys	–9.0	–7.8	–7.0	–7.5	–	–
	NH Asn/Ser	–19	–15.2	–30	–15	–15	–20

[a]50 mM phosphate buffer at pH 7.5 and 298 K.
[b]50 mM phosphate buffer at pH 5.2 and 295 K.
[c]10 mM phosphate buffer at pH 8.0 and 278 K.
[d]50 mM phosphate buffer at pH 6.0 and 301 K.
[e]100 mM Tris-HCl at pH 8.0 and 298 K.
[f]100 mM acetate buffer at pH 5.5 and 296 K.

In all blue copper proteins studied so far, the histidine signals display similar spectral features, whereas those of the resonances corresponding to the cysteine and axial ligand(s) vary among different proteins, reflecting changes in the electronic structure of the metal site. We have shown that in classic blue sites, the Cu(II)–Cys interaction depends on the axial ligand(s) strength [20]: a stronger axial ligand (such as in stellacyanin) reduces the Cu(II)-S_{Cys} covalence, thus giving rise to a sizably smaller electron spin density on the β-CH_2 Cys protons. In a nondistorted site, the contact shifts of the β-CH_2 protons of the Cu-bound Cys is expected to follow a Karplus-like sine-squared dependent function [19,43]. In tetragonally perturbed blue copper centers, such as those present in pseudoazurin and rusticyanin, the electron spin density on the Cys ligand is reduced when compared to plastocyanin and azurin, reflecting the different orientation of the Met residue [44]. In these, it appears that the average chemical shift of the β-CH_2 Cys relates well with the tilt of the Cu(II)-S_{Met} conjunction with respect to the ideal plane containing the three S_{Cys}–N_{His}–N_{His} atoms [23].

INVERSE DETECTED HETERONUCLEAR NMR SPECTROSCOPY: THE STRUCTURE OF Cu(II) PLASTOCYANIN

The progresses made in the investigation of blue copper proteins led to the determination of the solution structure of Cu(II) plastocyanin from *Synecchocystis* sp. PCC 6803, which represents the first solution structure of a paramagnetic, oxidized copper protein [26]. This was achieved on a ^{15}N-labeled protein by using standard 2D and 3D heteronuclear NMR experiments that were tailored to the fast relaxing signals of nuclei in the vicinities of the metal site. The resulting structure is well defined, with an RMSD from the mean structure for the solution structure family of 0.72 ± 0.14 and 1.16 ± 0.17 Å for backbone and heavy atoms, respectively. In Table 2, the relevant data on the structure (Protein Data Bank ID 1J5C) are reported, as well as the summary of the number and type of constraints used.

Table 2 Summary of NMR constraints used for structure calculation and structural quality parameters for oxidized and reduced plastocyanin from *Synechocystis sp*. PCC 6803 [26,45].

Structural constraints	Oxidized	Reduced
	Total	Total
Meaningful NOESY	1041	1344
1D NOE	18	0
Overall interesidue	162	209
Overall sequential	273	311
Overall medium-range	130	178
Overall long-range	494	646
R_1	26	0
ϕ	49	64
ψ	47	52
χ_2	1	0
H-bonds	18	19
Copper–ligand distances	4	4
Overall total	1204	1483
Target function (Å^2)	0.66	0.38
RMSD backbone atoms (Å)	0.72 ± 0.14	0.55 ± 0.07
RMSD heavy atoms (Å)	1.16 ± 0.17	1.14 ± 0.07

The dihedral angles of the Cu-βCH_2 of the bound Cys residue were constrained between 150° and 210° according to a sine-squared dependent relation, as established from the observed contact shifts of the corresponding resonances [19]. The observation of the large hyperfine contact shifts on signals A-F allowed us to impose also four experimentally validated coordination bond constraints.

For structure refinement relaxation, rate-derived upper distance limits were used. These were obtained by measuring the difference in nuclear longitudinal relaxation rate in the oxidized form with respect to the reduced one. This difference can indeed be related to metal-nucleus distance according to the Solomon equation [7], taking into account the possible contribution of other relaxation mechansims*:

$$R_{1\text{para}} = \frac{2}{15}\left(\frac{\mu_0}{4\pi}\right)\frac{\gamma_I^2 g_e^2 \mu_B^2 S(S+1)}{r^6}\left[\frac{\tau_c}{1+(\omega_I-\omega_S)^2\tau_c^2}+\frac{3\tau_c}{1+\omega_I^2\tau_c^2}+\frac{6\tau_c}{1+(\omega_I-\omega_S)^2\tau_c^2}\right]$$

where γ_I is the nuclear gyromagnetic ratio, g_e is the free electron g factor, S is the quantum number associated to the electron spin, r is the electron-nucleus distance, ω_I and ω_S are the Larmor frequencies of the nucleus and of the electron, respectively, and τ_c is the effective correlation time for the dipole–dipole interaction ($1/\tau_c = 1/\tau_s + 1/\tau_M + 1/\tau_r$, where τ_s is the electronic correlation time, τ_M is the exchange correlation time and τ_r is the rotational correlation time) and the other symbols have they usual meaning.

The paramagnetic contribution to the proton relaxation rate was extracted from the data by subtracting the diamagnetic component from the observed R_1. The diamagnetic contribution was estimated considering the average of all the relaxation rates relative to protons located far away from the copper ion. The distance between the copper ion and each proton for which the paramagnetic relaxation rate could be determined was established using a structure calculated without these constraints. A plot of

*Other mechanisms are Curie relaxation [65,66], often negligible in medium-sized copper protein with S = 1/2, and the Fermi contact relaxation [67], present only for the nuclei of metal-bound residues.

that distances vs. the 1/6 square of the relaxation times allowed the identification of a region of points delimited by two straight lines passing through the origin. The two limiting values for the slopes were then used to set the lower and upper distance limits for each proton [26].

The availability of the refined structure allowed the comparison with the solution structure of the reduced form [45], revealing no significant structural changes in the protein upon the redox process. Analysis of the ^{1}H and ^{15}N chemical shift changes in this region indicates that minor conformational rearrangement may occur between the two redox states.

Mobility studies were then performed on both reduced and oxidized plastocyanin [45]. This comparison confirmed that plastocyanin is a rigid molecule in both redox states, in the sub-millisecond time scale, consistent with a β-barrel structure. On the other hand, in the milliseconds and longer time scales, it shows significant protein flexibility on the loops connecting the β-strands, region that contains three (the Cys and the two His) of the four copper ligands.

DIRECT DETECTED HETERONUCLEAR NMR SPECTROSCOPY: THE STRUCTURE OF Cu(II) CopC

In the previous section we have shown how it is possible to obtain a wealth of structural and dynamical information on Type I Cu(II)-protein. However, when going to proteins containing Type II copper the electronic relaxation times of the metal ion are as such that the proton signals of residues close to the paramagnetic center become broad beyond detectable limit. This effect limits considerably the applicability of ^{1}H NMR spectroscopy and prompted us in exploring less conventional NMR approaches involving heteronuclei for the investigation of these challenging systems. Carbon-13 direct detection offers advantages in paramagnetic systems as the dipolar contributions to nuclear relaxation depend on the square of the gyromagnetic ratio of the observed nucleus and going from ^{1}H to ^{13}C detection a decrease in relaxation rates of a factor of about 16 occurs. Of course, there is a concomitant reduction in sensitivity, but this limitation can be overcome with the use of high field spectrometers as well as hardware specifically designed for heteronuclear observation [46–48].

Table 3 Summary of NMR constraints used for structure calculation and structural quality parameters for oxidized CopC from *Pseudomonas syringae* [56].

Structural constraints	Oxidized
	Total
Meaningful NOESY	1276
Overall interesidue	240
Overall sequential	364
Overall medium-range	88
Overall long-range	584
R_1	23
ϕ	83
ψ	52
χ_2	52
H-bonds	41
Copper–ligand distances	27
Target function ($Å^2$)	0.56
RMSD backbone atoms (Å)	1.07 ± 0.27
RMSD heavy atoms (Å)	1.58 ± 0.32

Several applications of ^{13}C direct detection to macromolecules have recently appeared in the literature [46,49–55]. Two-dimensional ^{13}C-^{13}C correlation experiments have been used to detect resonances in paramagnetic systems of nuclei at distances from the metal ion where the ^{1}H resonances were broadened beyond detectable limits [49,51–54]. It has been used also to detect and assign side chain correlations in an octameric protein [55] that, having a large molecular mass, suffers from similar problems of fast nuclear relaxation as paramagnetic systems do. We have extended this approach to obtain the solution structure of Cu(II) CopC from *Pseudomonas syringae* [56], a periplasmic protein capable of binding Cu(I) and Cu(II) at two different sites and involved in copper trafficking and homeostasis in gram-negative bacteria (Fig. 5) [57,58].

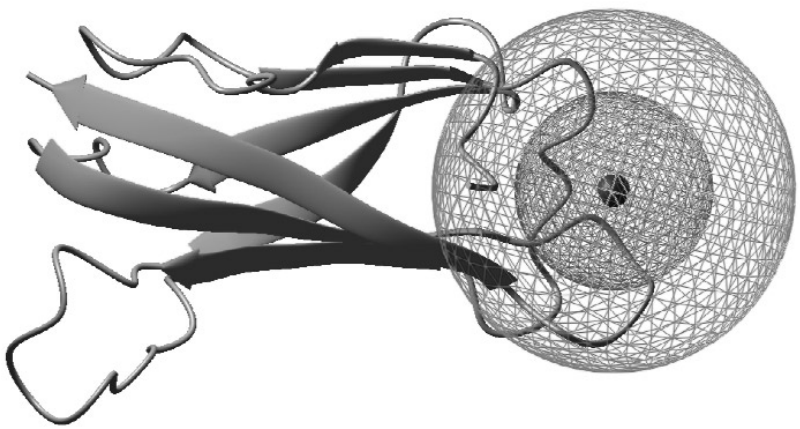

Fig. 5 Ribbon drawing of Cu(II)–CopC from *Pseudomonas syringae* showing the secondary structure elements of the protein (PDB ID 1OT4, Model 1). The metal ion is represented as a black sphere of arbitrary dimension. The detection limits through NMR are shown as concentric dashed spheres centered on the copper ion. The outer sphere of 11 Å radius represents the region in which ^{1}H-detected experiments are not fruitful, while using experiments based on heteronuclear detection the "blind" zone restricts to the inner sphere of 6 Å radius. The picture was rendered with Molmol 2.2.

The structure of the apo- [59] and of the Cu(I)-forms [60] of this protein have been solved by us recently, but when standard experiments based on ^{1}H detection are performed on Cu(II)CopC, resonances of almost all the residues within about 11 Å from the potential copper binding site disappear (Fig. 5) [59]. Another set of signals from residues in the borderline region are still detectable in standard spectra, but they experience variable broadening that makes it difficult to assign them using standard triple-resonance NMR protocols [59].

Our first concern was the identification of broad signals underneath diamagnetic signals. Several saturation-recovery spectra obtained with increasing recovery delays clearly show a small number of signals that recover much faster than all the others (Fig. 6A). The selectivity of these experiments is further improved by appropriate linear combination of two 1D experiments recorded with different recovery delays. In this way, it is possible to further suppress slower relaxing signals, enhancing the detection of the fast-relaxing ones (Fig. 6B).

Acquiring ^{13}C-^{13}C CT-COSY experiments with different CT delays (Figs. 7A,B), optimized either to detect Cα-Cβ connectivities or Cα-CO backbone connectivities, ^{13}C-^{13}C COCAMQ and ^{13}C-^{15}N CONSQC (Fig. 7C) experiments, 37 ^{13}C and 11 ^{15}N nuclei not detected in standard experiments were identified and assigned. In total, about 85 % of carbon atoms and 95 % of nitrogen atoms were assigned, representing a substantial increase with respect to the standard approach (limited to 76 % and 83 %, respectively). Only 3 residues remained unidentified. These residues are thus likely to be the

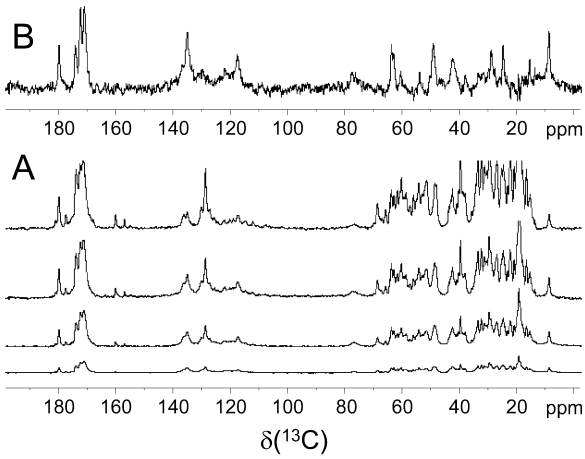

Fig. 6 (A) Saturation recovery 1D ^{13}C spectra recorded with different recovery delays (from bottom to top 8, 16, 32, 128 ms). Experiments with shorter recovery delays were acquired with an increasing number of scans to maintain a good signal-to-noise ratio (64k, 32k, 8k, 2k scans for the experiments with recovery delays of 8, 16, 32, 128 ms, respectively). The spectra are rescaled according the number of scans to have comparable signal intensities. (B) The difference spectrum between the experiments with 32 and 128 ms recovery delays. The experiments were performed at 16.4 T with a spectrometer operating at 176.1 MHz for carbon.

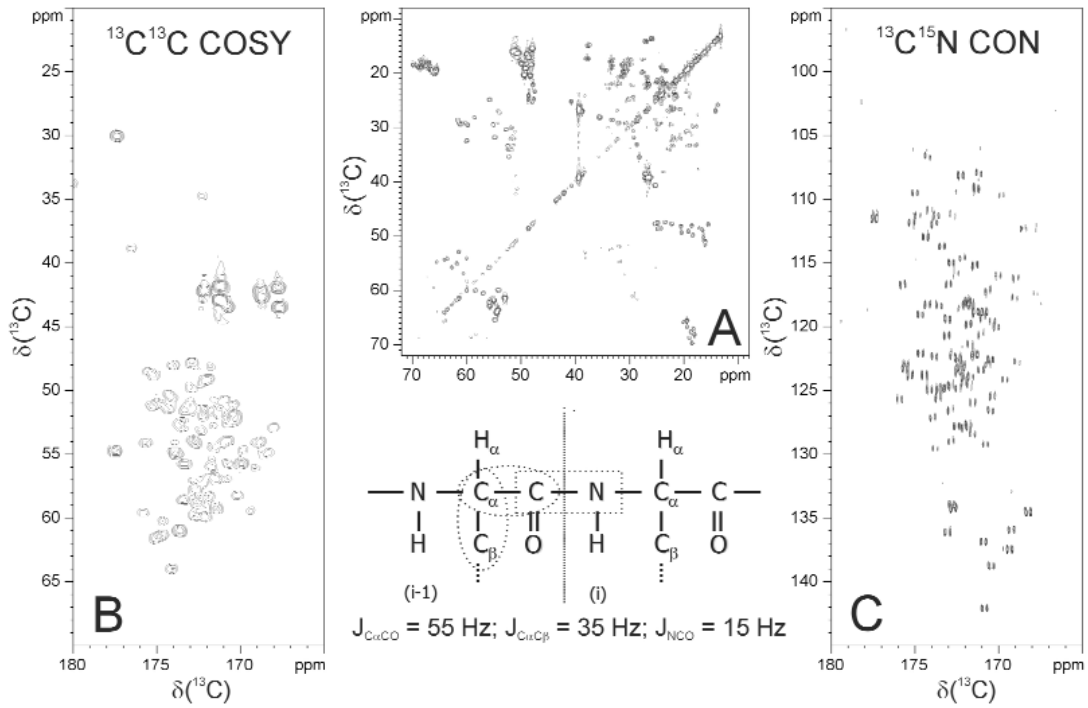

Fig. 7 Selected regions of 2D heterenoculear experiments recorded at 16.4 T with a spectrometer operating at 176.1 MHz for carbon. (A) reports the CO-Cα region of a ^{13}C-^{13}C COSY experiment optimized to detect such connectivities while (B) reports the aliphatic region of a similar spectrum optimized to detect Cα-Cβ connectivities. (C) reports the correlation between backbone CO and N. The scheme of the main coupling constant involved in these spectra is reported for clarity.

Cu(II) ligands, that are expected to experience large Fermi contact contribution to the relaxation rates that makes them broad beyond detectable limits.

The 2D and 3D NOESY spectra provide 1777 NOEs which correspond to 1276 meaningful ^{1}H-^{1}H distances. Additional constraints were provided by 145 dihedral angles and 27 hydrogen bonds. Paramagnetism-based constraints were constituted by 23 metal-heteronucleus distances, obtained from longitudinal ^{13}C relaxation rates, and by 83 proton pseudocontact shifts. All these constraints were used in the program PSEUDYANA [61] to calculate the solution structure of the Cu(II)-CopC protein. The target function is 0.56 ± 0.07 Å^2 and the RMSD to the mean is 1.07 ± 0.27 Å and 1.58 ± 0.32 Å for backbone and all heavy atoms, respectively. The RMSD of the copper ion, which is only determined by the paramagnetism based constraints is 1.1 Å, demonstrating that ^{13}C longitudinal relaxation rates are very efficient in determining the position of the copper ion in the protein frame.

PERSPECTIVES

In the recent years the technological efforts in the field of NMR hardware development were devoted at increasing the sensitivity of proton-detected experiments. Indeed, almost all the heteronuclear experiments in structure determination protocols are based on reverse detection schemes, to exploit the larger proton sensitivity. On the other hand, these experiments suffer from proton transverse relaxation during the coherence transfer steps, and their application is limited by the nuclear relaxation properties of the system investigated. Most of the NMR experiments, however, could be performed using direct heteronuclear excitation and detection without involving protons at any place in the sequence. From the results presented, there is evidence that if the loss in sensitivity on passing from the proton to the heteronuclear scheme can be balanced by improved hardware performances, then the increase in detectability of signals close to the paramagnetic center is significant.

The presented approach, based on scalar-transfer based experiments, has a limit. Indeed, coherence transfer mechanisms become less effective as the linewidths of the signals approach the value of the scalar coupling constant used for the transfer. In case of one-bond carbon–carbon couplings, the $^{1}J_{CC}$ is fairly large (35–55 Hz), but it is evident that the paramagnetic R_2 contributions can easily overcome this range. This means that to detect significantly broad signals, alternative experimental schemes should be used. From Fig. 1, it is evident that the paramagnetic contribution to relaxation is much less effective on longitudinal rates compared to transverse rates. Therefore, experiments in which magnetization is stored along the z axis should be affected to a minor extent by paramagnetic relaxation. This is the case of ^{13}C-^{13}C NOESY experiments [62], which promise to become the choice experiment for the assignment of paramagnetic systems [47].

As it appear in Fig. 7, a pressing problem in 2D ^{13}C-^{13}C direct detection experiments is the large amount of carbon–carbon coupling constants that complicate the spectra. Indeed, the 35–55 Hz coupling constants are responsible for doublets or more complicated multiplet structures that dramatically reduce the effective resolution of the spectra. This becomes a severe drawback if we want to use ^{13}C spectroscopy to detect broad signals in crowded regions of the spectra such as it occurs for large molecules and for paramagnetic systems characterized by small hyperfine shifts such as Cu(II)-proteins. Band-selective homodecoupling can in part solve the problem making it possible to decouple CO from Cα (and Cβ eventually) resonances and vice versa, or to decouple the aliphatic carbons signals from carbonyl signals. This is sufficient to quench all the relevant carbon–carbon couplings in the ^{13}C-^{13}C COCAMQ spectrum and contributes a significant to essential simplification of the spectra in the aliphatic region [47]. This is a valid alternative to other available tools to quench such coupling [63].

CONCLUDING REMARKS

The characterization of proteins in solution through NMR provides a wealth of information, including protein mobility, factors affecting stability and the fold–unfold process and ultimately, the solution

structure. Technological advances in NMR instrumentation, including the development of the methodological tools, are extending the number of proteins that can be characterized through NMR spectroscopy. After the successful determination of the solution structure of the Cu(II) CopC from *Pseudomonas syringae* [56], it is apparent that the methods and the results typical of diamagnetic proteins can be obtained also for paramagnetic Cu(II) proteins. In addition, the presence of the paramagnetic center can be exploited to obtain information on the electronic properties of the system through analysis of contact and pseudocontact shifts, as well as nuclear relaxation parameters [64]. The very same parameters can be exploited to set structural constraints, essential for defining the details of the structure around the active center without any geometrical assumption derived from other techniques.

This technological and methodological challenge represented by the "protonless" approach may lead to a breakthrough in the application of NMR spectroscopy to paramagnetic proteins but, most important, to all the systems that suffers from fast transverse relaxation such as large molecular mass proteins and protein–protein adducts.

REFERENCES

1. I. Bertini, A. Sigel, H. Sigel. *Handbook on Metalloproteins*, Marcel Dekker, New York (2001).
2. J. J. R. Frausto da Silva and R. J. P. Williams. *The Biological Chemistry of the Elements: The Inorganic Chemistry of Life*, Oxford University Press, New York (2001).
3. I. Bertini and C. Luchinat. *NMR of Paramagnetic Molecules in Biological Systems*, Benjamin/Cummings, Menlo Park, CA (1986).
4. I. Bertini, C. Luchinat, G. Parigi. *Solution NMR of Paramagnetic Molecules*, Elsevier, Amsterdam (2001).
5. L. Banci, I. Bertini, R. Del Conte, S. Mangani, W. Meyer-Klaucke. *Biochemistry* **8**, 2467 (2003).
6. L. Banci, I. Bertini, C. Luchinat. *Nuclear and Electron Relaxation. The Magnetic Nucleus-unpaired Electron Coupling in Solution*, VCH, Weinheim (1991).
7. I. Solomon. *Phys. Rev.* **99**, 559 (1955).
8. L. Banci, R. Pierattelli, A. J. Vila. *Adv. Protein Chem.* **60**, 397 (2002).
9. D. W. Randall, D. R. Gamelin, L. B. LaCroix, E. I. Solomon. *J. Biol. Inorg. Chem.* **5**, 16 (2000).
10. A. M. Nersissian and E. Shipp. *Adv. Protein Chem.* **60**, 271 (2002).
11. S. H. Koenig and R. D. Brown III. *Progr. NMR Spectrosc.* **22**, 487 (1991).
12. S. J. Kroes, J. Salgado, G. Parigi, C. Luchinat, G. W. Canters. *JBIC* **1**, 551 (1996).
13. E. I. Solomon, M. J. Baldwin, M. D. Lowery. *Chem. Rev.* **92**, 521 (1992).
14. A. P. Kalverda, J. Salgado, C. Dennison, G. W. Canters. *Biochemistry* **35**, 3085 (1996).
15. C. O. Fernández, A. I. Sannazzaro, A. J. Vila. *Biochemistry* **36**, 10566 (1997).
16. A. J. Vila, B. E. Ramirez, A. J. Di Bilio, T. J. Mizoguchi, J. H. Richards, H. B. Gray. *Inorg. Chem.* **36**, 4567 (1997).
17. J. Salgado, S. J. Kroes, A. Berg, J. M. Moratal Mascarell, G. W. Canters. *J. Biol. Chem.* **273**, 177 (1998).
18. C. Dennison and T. Kohzuma. *Inorg. Chem.* **38**, 1491 (1999).
19. I. Bertini, S. Ciurli, A. Dikiy, R. Gasanov, C. Luchinat, G. Martini, N. Safarov. *J. Am. Chem. Soc.* **121**, 2037 (1999).
20. I. Bertini, C. O. Fernández, B. G. Karlsson, J. Leckner, C. Luchinat, B. G. Malmström, A. M. Nersissian, R. Pierattelli, E. Shipp, J. S. Valentine, A. J. Vila. *J. Am. Chem. Soc.* **122**, 3701 (2000).
21. C. Dennison and A. T. Lawler. *Biochemistry* **40**, 3158 (2001).
22. K. Sato and C. Dennison. *Biochemistry* **41**, 120 (2002).
23. A. Donaire, B. Jimenez, C. O. Fernandez, R. Pierattelli, T. Niizeki, J. M. Moratal, J. F. Hall, T. Kohzuma, S. S. Hasnain, A. J. Vila. *J. Am. Chem. Soc*. **124**, 13698 (2002).
24. K. Sato, T. Kohzuma, C. Dennison. *J. Am. Chem. Soc.* **125**, 2101 (2003).

25. C. Dennison, M. D. Harrison, A. T. Lawler. *Biochem. J.* **371**, 377 (2003).
26. I. Bertini, S. Ciurli, A. Dikiy, C. O. Fernández, C. Luchinat, N. Safarov, S. Shumilin, A. J. Vila. *J. Am. Chem. Soc.* **123**, 2405 (2001).
27. E. I. Solomon, U. M. Sundaram, T. E. Machonin. *Chem. Rev.* **96**, 2563 (1996).
28. V. Clementi and C. Luchinat. *Acc. Chem. Res.* **31**, 351 (1998).
29. I. Bertini, K. L. Bren, A. Clemente, J. A. Fee, H. B. Gray, C. Luchinat, B. G. Malmström, J. H. Richards, D. Sanders, C. E. Slutter. *J. Am. Chem. Soc.* **46**, 11658 (1996).
30. C. Luchinat, A. Soriano, K. Djinovic-Carugo, M. Saraste, B. G. Malmström, I. Bertini. *J. Am. Chem. Soc.* **119**, 11023 (1997).
31. J. Salgado, G. Warmerdam, L. Bubacco, G. W. Canters. *Biochemistry* **37**, 7378 (1998).
32. C. Dennison, E. Vijgenboom, S. de Vries, J. Van der Oost, G. W. Canters. *FEBS Lett.* **365**, 92 (1995).
33. R. C. Holz, M. L. Alvarez, W. G. Zumft, D. M. Dooley. *Biochemistry* **38**, 11164 (1999).
34. L. Bubacco, J. Salgado, A. W. Tepper, E. Vijgenboom, G. W. Canters. *FEBS Lett.* **442**, 215 (1999).
35. L. Bubacco, E. Vijgenboom, C. Gobin, A. W. Tepper, J. Salgado, G. W. Canters. *J. Mol. Catal. B* **8**, 27 (2000).
36. C. O. Fernandez, J. A. Cricco, C. E. Slutter, J. H. Richards, B. H. Gray, A. J. Vila. *J. Am. Chem. Soc.* **123**, 11678 (2002).
37. A. G. Sykes. *Adv. Inorg. Chem.* 377 (1991).
38. E. T. Adman. *Adv. Protein Chem.* **42**, 144 (1991).
39. M. E. Murphy, P. F. Lindley, E. T. Adman. *Protein Sci*. **6**, 761 (1997).
40. A. Messerschmidt. *Struct. Bonding* **90**, 37 (1998).
41. A. J. Vila and C. O. Fernández. In I. Bertini, A. Sigel, H. Sigel (Eds.), *Handbook on Metalloproteins*, p. 813, Marcel Dekker, New York (2001).
42. L. Banci, I. Bertini, C. Luchinat, M. Piccioli, A. Scozzafava, P. Turano. *Inorg. Chem.* **28**, 4650 (1989).
43. I. Bertini, F. Capozzi, C. Luchinat, M. Piccioli, A. J. Vila. *J. Am. Chem. Soc.* **116**, 651 (1994).
44. L. B. LaCroix, D. W. Randall, A. M. Nersissian, C. W. G. Hoitink, G. W. Canters, J. S. Valentine, E. I. Solomon. *J. Am. Chem. Soc.* **120**, 9621 (1998).
45. I. Bertini, D. A. Bryant, S. Ciurli, A. Dikiy, C. O. Fernández, C. Luchinat, N. Safarov, A. J. Vila, J. Zhao. *J. Biol. Chem.* **276**, 47217 (2001).
46. Z. Serber, C. Richter, D. Moskau, J.-M. Boehlen, T. Gerfin, D. Marek, M. Haeberli, L. Baselgia, F. Laukien, A. S. Stern, J. C. Hoch, V. Doetsch. *J. Am. Chem. Soc.* **122**, 3554 (2000).
47. W. Bermel, I. Bertini, I. C. Felli, R. Pierattelli, R. Kümmerle. *J. Am. Chem. Soc.* **125**, 16423 (2003).
48. I. Bertini, I. C. Felli, R. Kümmerle, D. Moskau, R. Pierattelli. *J. Am. Chem. Soc.* **126**, 464 (2004).
49. U. Kolczak, J. Salgado, G. Siegal, M. Saraste, G. W. Canters. *Biospectroscopy* **5**, S19 (1999).
50. Z. Serber, C. Richter, V. Dötsch. *ChemBioChem* **2**, 247 (2001).
51. I. Bertini, Y.-M. Lee, C. Luchinat, M. Piccioli, L. Poggi. *ChemBioChem* **2**, 550 (2001).
52. T. C. Pochapsky, S. S. Pochapsky, T. Ju, H. Mo, F. Al-Mjeni, M. J. Maroney. *Nat. Struct. Biol*. **9**, 966 (2002).
53. T. E. Machonkin, W. M. Westler, J. L. Markley. *J. Am. Chem. Soc.* **124**, 3204 (2002).
54. M. Kostic, S. S. Pochapsky, T. C. Pochapsky. *J. Am. Chem. Soc.* **124**, 9054 (2002).
55. A. Eletsky, O. Moreira, H. Kovacs, K. Pervushin. *J. Biomol. NMR* **26**, 167 (2003).
56. F. Arnesano, L. Banci, I. Bertini, I. C. Felli, C. Luchinat, A. R. Thompsett. *J. Am. Chem. Soc.* **125**, 7200 (2003).
57. D. A. Cooksey. *FEMS Microb. Rev.* **14**, 381 (1994).
58. S. Silver. *Gene* **179**, 9 (1996).

59. F. Arnesano, L. Banci, I. Bertini, A. R. Thompsett. *Structure* **10**, 1337 (2002).
60. F. Arnesano, L. Banci, I. Bertini, S. Mangani, A. R. Thompsett. *Proc. Natl. Acad. Sci. USA* **100**, 3814 (2003).
61. L. Banci, I. Bertini, M. A. Cremonini, G. Gori Savellini, C. Luchinat, K. Wüthrich, P. Güntert. *J. Biomol. NMR* **12**, 553 (1998).
62. M. W. F. Fisher, L. Zeng, E. R. P. Zuiderweg. *J. Am. Chem. Soc.* **118**, 12457 (1996).
63. N. Shimba, A. S. Stern, C. S. Craik, J. C. Hoch, V. Dötsch. *J. Am. Chem. Soc.* **125**, 2382 (2003).
64. I. Bertini, C. Luchinat, M. Piccioli. *Methods Enzymol.* **339**, 314 (2001).
65. M. Gueron. *J. Magn. Reson.* **19**, 58 (1975).
66. A. J. Vega and D. Fiat. *Mol. Phys.* **31**, 347 (1976).
67. I. Solomon and N. Bloembergen. *J. Chem. Phys.* **25**, 261 (1956).